Acta metall. Vol. 33, No. 2, pp. 213–229, 1985
Printed in Great Britain.

0001-6160/85 $3.00 + 0.00
Pergamon Press Ltd

EFFECT OF BORON ON GRAIN-BOUNDARIES IN Ni_3Al†

C. T. LIU, C. L. WHITE and J. A. HORTON
Metals and Ceramics Division, Oak Ridge National Laboratory, Oak Ridge, TN 37830, U.S.A.

(*Received* 14 *May* 1984; *in revised form* 17 *August* 1984)

Abstract—The effects of boron additions (up to 0.4 wt% B) on grain-boundary chemistry and tensile properties of Ni_3Al containing 24–26 at.% Al were studied. Room-temperature ductility and fracture behavior of B-doped Ni_3Al depended critically on deviation from alloy stoichiometry. As the aluminum content of B-doped Ni_3Al is decreased below 25 at.%, the ductility increases dramatically and the fracture mode changes from intergranular to transgranular. Auger studies indicate that the intensity of boron segregation to grain boundaries increases and the concentration of grain-boundary aluminium decreases significantly with decreasing bulk aluminum concentration. These results suggest that alloy stoichiometry strongly influences grain-boundary chemistry which in turn, affects the grain-boundary cohesion. Boron exhibits an unusual segregation behavior in Ni_3Al, i.e. it has a strong tendency to segregate to the grain boundaries but not to cavity (free) surfaces. On the other hand, sulfur, an embrittling impurity, tends to segregate more strongly to free surfaces than to grain boundaries. The beneficial effect of boron is in agreement with existing theories of solute segregation effects on grain-boundary cohesion. The yield stress of B-doped Ni_3Al decreases with increasing grain size produced by long-term annealing at 1000°C. The yield stress obeys the Hall-Petch relation: $\sigma_y = \sigma_{o,y} + k_y d^{-1/2}$ with $\sigma_{o,y} = 163$ MPa and $k_y = 8.2$ MPa cm$^{1/2}$. The tensile elongation was initially independent of grain size, and showed only a moderate decrease from about 50–40% with grain diameters larger than 110 μm.

Résumé—Nous avons étudié l'influence d'additions de bore (jusqu'à 0,4% de bore en poids) sur la chimie des joints de grains et les propriétés en traction de Ni_3Al contenant de 24 à 26 at.% Al. La ductilité et la rupture à la température ambiante de Ni_3Al dopé au bore dépendent de manière critique de la déviation par rapport à la stoechiométrie. Lorsqu'on diminue la teneur en aluminium de Ni_3Al dopé au bore audessons de 25 at.% la ductilité augmente considérablement et le mode de rupture panc d'intergranulaire à transgranulaire. Des études par spectroscopie Auger ont montré que la quantité de bore ségrégé aux joints de grains augmente et que la concentration d'aluminium intergranulaire diminue/notablement lorsqu'on diminue la concentration en masse d'aluminium. Ces résultats suggèrent une forte influence de la stoechiométrie de l'alliage sur la chimie du joint de grains qui, à son tour, modifie la cohésion intergranulaire.

Le bore ségrège de maniège inhabituelle dans Ni_3Al, car il a une forte tendance à ségrèger sur les joints de grains, mais non sur la surface (libre) des cavités. Par contre, le soufre, qui est une impureté fragilisante, a tendance à ségrèger plus sur les surfaces libres que sur les joints de grains. L'effet bénéfique du bore est en accord avec les théories existantes sur les effets de la ségrégation de soluté sur la cohésion intergranulaire.

La limite élastique de Ni_3Al dopé au bore diminue lorsqu'on augmente la taille de grains par un long revenu à 1000°C. La limite élastique vérifie la relation de Hall et Petch: $\sigma_y = \sigma_{0,y} + k_y d^{-1/2}$, où $\sigma_{0,y} = 163$ MPa et $k_y = 8{,}2$ MPa cm$^{1/2}$. L'allongement en traction ne dépendait initialement pas de la taille des grains et il ne diminuait que modérément, d'environ 50 à 40% pour une taille de grains supérieure à 110 μm

Zusammenfassung—Der Einfluß von Borzugaben bis zu 0,4 Gew.-% zu Ni_3Al (Al-Gehalt 24 bis 26 At.-%) au die chemische Zusammensetzung au Korngrenzen und auf das Verhalten unter Zugbelastung wurde untersucht. Duktilität und Bruchverhalten hängen bei Raumtemperatur im B-dotierten Ni_3Al kritisch von der Stöchiometrieabweichung ab. Bei einem Al-Gehalt unter 25 At.-% ist die Duktilität drastisch erhöht und die Bruchmode wechselt von inter- zu transgranular. Aus Augeruntersuchungen ergab sich, daß die Borsegregation an den Korngrenzen zunimmt und die Al-Konzentration dort mot abnehmender Al-Volumkonzentration beträchlich kleiner wird. Diese Ergebnisse legen nahe, daß die Stöchiometrie der Legierung die Chemie an der Korngrenze erheblich beeinflußt und diese wiederum die Korngrenzkohäsion. Bor zeigt in Ni_3Al ein ungewöhnliches Segregationsverhalten: eine starke Neigung zur Segregation an Korngrenzen, nicht jedoch freien und Hohlraumoberflachen. Andererseits segregiert das versprödende Element Schwefel eher an freien Oberflächen als an Korngrenzen. Der günstige Einfluß des Bors stimmt mit Theorient zum Einfluß der Segregation auf die Korngrenzkohäsion übrein. Die Fließspannung des Bor-dotierten Ni_3Al sinkt mit zunehmender Korngröße (hergestellt durch langes Glühen bei 1000°C) ab. Sie gehorcht der Hall-Petch-Beziehung $\sigma_y = \sigma_{0,y} + k_y d^{-1/2}$ mit $\sigma_{0,y} = 163$ MPa und $k_y = 8{,}2$ MPa$\sqrt{\text{cm}}$. Die erreichbare Dehung hing bei kleineren Korngrößen nicht von der Korngröße ab und wurde bei Korndurchemessern oberhalb 110 μm nur langsam kleiner.

INTRODUCTION

The nickel aluminide, Ni_3Al, is an intermetallic compound having the $L1_2$ ordered crystal structure (sim-

†Research sponsored by the Division of Materials Sciences, U.S. Department of Energy under contract DE-AC05-8421400 with the Martin Marietta Energy Systems, Inc.

ilar to Cu_3Au) below the peritectic temperature (1395°C) [1]. The aluminide has unique properties that make it attractive for structural applications at elevated temperatures. Unlike disordered alloys, the yield strength of Ni_3Al increases with increasing test temperature [2–4]. The aluminide is the most important strengthening constituent (γ' phase) of commercial nickel-base superalloys. It tends to form adherent aluminum oxide scales that protect the base material from excessive oxidation and corrosion [5, 6]. In addition, its density is significantly lower than that of commercial superalloys.

The major difficulty with Ni_3Al as an engineering material, however, is its tendency for low ductility and brittle fracture in polycrystalline forms [7–9]. This brittleness effectively precludes its fabrication into useful structural components. It has been known for years that single crystals of Ni_3Al are ductile but its polycrystalline forms are extremely brittle [7–11]. The brittleness of such polycrystals is associated with grain-boundary weakness that causes brittle intergranular fracture without appreciable plastic deformation within the grains. Recent studies of grain-boundary chemistry by White and Stein [12] revealed that sulfur, a trace impurity in Ni_3Al, has a strong tendency to segregate and possibly embrittles the grain boundaries. Oxygen and carbon were also detected on the boundaries, but were thought to be a result of contamination by the residual atmosphere in the Auger system.

Microalloying processes have been used to alleviate the brittle intergranular fracture in Ni_3Al. Microalloying involves addition of small concentrations of dopants (usually in ppm range) to control chemistry and cohesion of grain boundaries. Various dopants were added to Ni_3Al [6, 13, 14], including boron, carbon, titanium, cerium, calcium, magnesium, manganese, and silicon. Among these dopants, boron was found to be the most effective in improving fabricability and ductility of Ni_3Al. Aoki and Izumi [13] first discovered the beneficial effect of boron in Ni_3Al and observed a tensile ductility of 35% elongation at room temperature. By control of boron concentration and thermomechanical treatment in Ni_3Al, Liu and Koch [6] reported a tensile elongation exceeding 50%—the highest tensile ductility ever achieved by polycrystalline aluminides. Manganese additions were found [14] to further improve the fabricability of B-doped Ni_3Al.

In this paper, we report on an extensive study of B-doped Ni_3Al. We have investigated the effects of boron concentration, alloy stoichiometry, and microstructure on its strength and ductility. The principal objective of this study is to understand the basic role of boron on ductilization of Ni_3Al. The ductility and fracture behavior of B-doped Ni_3Al containing 24 and 26 at.% Al were characterized by tensile tests at room temperature, and were correlated with grain-boundary chemistry and structural features as determined by Auger electron spectroscopy (AES), scanning electron microscopy (SEM), and transmission electron microscopy (TEM). Emphasis is placed on understanding the chemical aspects of boron on the composition and cohesion of grain boundaries in Ni_3Al.

EXPERIMENTAL

Nickel aluminides containing 24–26 at.% Al (12.7–13.9 wt% Al) were doped with 0.005, 0.01, 0.025, 0.04, 0.05, 0.07, 0.1, 0.2 and 0.4 wt% B (0.02–1.9 at.% B). The B-doped aluminides were prepared by arc melting and drop casting, using pure nickel and aluminium metals and a master alloy of Ni–4 wt% B. The nominal compositions of the aluminides were calculated based on the formula $(Ni_3Al)_{1-x}B_x$ where x is the weight percent of boron. The drop-casting technique was used here to refine ingot grain structure and reduce compositional segregation during solidification. The cast ingots were homogenized for 5-h at 1000°C, and then fabricated into sheets by repeated rolling at room temperature, with intermediate anneals at 1000/1050°C. The alloy compositions were determined by wet chemistry, and spark-source mass spectroscopic (SSMS) analyses. Quantitative electron microprobe analyses of second-phase particles observed in B-doped Ni_3Al were performed using a JEOL electron superprobe.

The microstructures of B-doped Ni_3Al annealed for various times at 1000°C in vacuum were examined metallographically. The samples were polished by standard techniques and etched in a solution of 20 H_2O, 20 HNO_3, 10 HF, 20 H_3PO_4, 10 acetic acid, and 10 HCl by-parts. The microhardness of selected samples was measured using a Shimadzu hardness tester with a 1000-g load and a holding time of 15 s. The crystal structure of B-doped Ni_3Al was examined by X-ray diffraction, using CuK_α radiation.

Sheet specimens with a gage section of $12.7 \times 3.2 \times 0.7$ mm were used for measurement of tensile properties at room temperature. Tensile tests were conducted on an Instron testing machine at a strain rate $9.2 \times 10^{-7}\,s^{-1}$. The load–time curves were recorded on a strip chart, from which tensile data were calculated. The fracture surfaces were examined by optical microscopy and SEM.

Auger electron spectroscopy (AES) was used to analyze intergranular fracture surfaces of B-doped and undoped Ni_3Al. The application of AES to the study of grain-boundary segregation is discussed at length elsewhere [15, 16] and only details pertinent to this study are presented here. Specimens were fractured in situ by impact bending at a pressure of $< 2 \times 10^{-8}$ Pa. When necessary (normally with B-doped specimens containing < 24.5 at.% Al), specimens were severely notched and the fracture device was cooled with flowing liquid nitrogen to promote intergranular fracture. Fracture surfaces were imaged using secondary electrons, and features less than 1 μm in diameter could generally be resolved. Unless

otherwise noted, a primary beam energy of 5 keV was used. In all cases, intergranular and transgranular portions of the fracture surface were easily distinguished. Where appropriate, elemental mapping (using Auger peak intensities to modulate image brightness) was employed.

Following AES analysis of the fractured specimens, they were sputter etched using 5 keV argon ions at a current density of $\sim 0.22\ Am^{-2}$ to remove the topmost atoms from the fracture surface, and to expose the underlying material for analysis [17]. For the conditions in our experiments, we estimated an etching rate of $1.4–4.1 \times 10^{-11}$ m/s (0.8–2.4 nm/min).

Structural features in undoped and B-doped Ni_3Al samples were examined in transmission using a Philips EM 400T equipped with a field-emission gun and a JEM 120CX analytical transmission electron microscopes. Disks of about 3 mm dia were cut from Ni_3Al sheets and electrochemically thinned in a solution of 70% ethanol alcohol, 10% butyl cellusolve, 12.5% distilled water, and 7.5% perchloric acid at $-10°C$. Compositions of second-phase particles were also determined by energy dispersive spectroscopy (EDS/TEM).

RESULTS

Alloy fabrication and chemical composition

Undoped Ni_3Al aluminides containing 24 and 26 at.% Al cracked badly during cold fabrication. All cracks were formed intergranularly, indicating the brittleness of grain boundaries in Ni_3Al. The aluminides doped with 0.05 and 0.1 wt% B can be fabricated into sheets; however, their fabricability strongly depends on the aluminum concentration. The 24 at.% Al aluminides were readily rolled into sheet stock by repeated cold rolling with intermediate anneals at 1000/1050°C. The initial rolling involved a reduction in thickness of 12–15%, which was gradually increased to 30% between each intermediate anneal. Sheet fabrication became increasingly difficult as the aluminum content was increased; aluminides with greater than 25 at.% Al (i.e. Al-rich deviations from stoichiometry) could not be successfully fabricated into 0.76 mm sheets by cold rolling.

The effect of boron concentration on fabricability was determined using a series of Ni_3Al aluminides with 24 at.% Al. The aluminides doped with 0.01 wt% B or less cracked during cold fabrication. The 0.025% B aluminide was fabricated into sheet stock; however shallow surface cracks were observed during early stages of fabrication. The aluminides with 0.04 and 0.2% B were fabricated into good-quality sheets, but the aluminide with 0.4% B cracked during fabrication.

Table 1 shows the chemical compositions of undoped and B-doped Ni_3Al aluminides with 24 at.% Al. The major elements were determined by volumetric or gravimetric analysis, trace impurities were determined by SSMS, and interstitials were determined by vacuum fusion and Leco Carbon analyses. The boron concentrations agree well with nominal compositions indicating no major difficulty in controlling the boron dopant in the aluminides. The nickel levels obtained from chemical analyses are also in good agreement with the nominal compositions, although the analyzed values are consistently lower. The close agreement is expected because there was no appreciable loss of weight during arc melting. Trace impurities and interstitial contents both are very low in the aluminides. For example, the sulfur level is less than 1–3 ppm, and the total oxygen and carbon contents are less than 160 ppm (by weight).

Table 1. Chemical analysis of B-doped and undoped Ni_3Al (24 at.% Al)

	Composition wt%							
	IC-2		IC-15		IC-6		IC-36	
Element	Nominal	Analyzed	Nominal	Analyzed	Nominal	Analyzed	Nominal	Analyzed
Ni[a]	87.32	86.83	87.28	87.18	87.23	87.03	87.15	86.92
Al	12.68	Balance	12.67	Balance	12.65	Balance	12.65	Balance
B[b]	0.00	<0.0004	0.05	0.048	0.10	0.094	0.20	0.193
Hf[c]		<0.0005		<0.0005		<0.0005		<0.0005
Zr[c]		<0.0001		<0.0001		<0.0001		<0.0001
Cu[c]		0.0001		0.0001		0.0001		0.0001
Co[c]		<0.0001		≤0.0001		<0.0001		≤0.0001
Fe[c]		0.0010		0.0003		0.0003		0.0003
Mn[c]		≤0.0001		≤0.0001		≤0.0001		≤0.0001
Ca[c]		<0.0001		<0.0001		<0.0001		<0.0001
S[c]		<0.0001		<0.0003		<0.0001		<0.0003
P[c]		Masked		Masked		Masked		Masked
Si[c]		≤0.0003		≤0.0003		≤0.0003		≤0.0003
Mg[c]		≤0.0005		<0.0005		≤0.0005		<0.0005
Au[c]		<0.0003		<0.0003		<0.0003		<0.0003
Ce[c]		<0.0003		<0.0003		<0.0003		≤0.0003
O[d]		0.0050		0.0154		0.0024		0.0133
C[e]		0.0023		0.0042		0.0037		0.029

[a]Gravimetric analysis.
[b]Volumetric analysis.
[c]Spark-source mass spectroscopic analysis (SSMS).
[d]Vacuum fusion analysis.
[e]Leco carbon analysis.

Microstructure and second phase

Figure 1 shows optical microstructures of Ni_3Al (24 at.% Al) doped with 0.1, 0.2 and 0.4 wt% B. The 0.1 and 0.2% B aluminides exhibit essentially single-phase structure, whereas second-phase particles appearing in a blocky form, are observed in the 0.4% B aluminide.

The second-phase particles were examined using TEM. The particles lie preferentially along low-angle boundaries and typically are very thin ($\sim 0.5\,\mu m$) in one dimension [Fig. 2(a)]. They have the $M_{23}B_6$ (or $M_{23}C_6$) crystal structure, which is an fcc tau phase with a lattice parameter 1.036 nm, as determined by selected-area-diffraction (SAD) [Fig. 2(b)]. This lattice parameter is 2.91 times that for the Ni_3Al matrix and yields a 3% misfit between particles and matrix. In general, these particles have a cube-on-cube orientation relationship with the matrix, which is expected when the misfit in lattice parameters is slightly less than 3%.

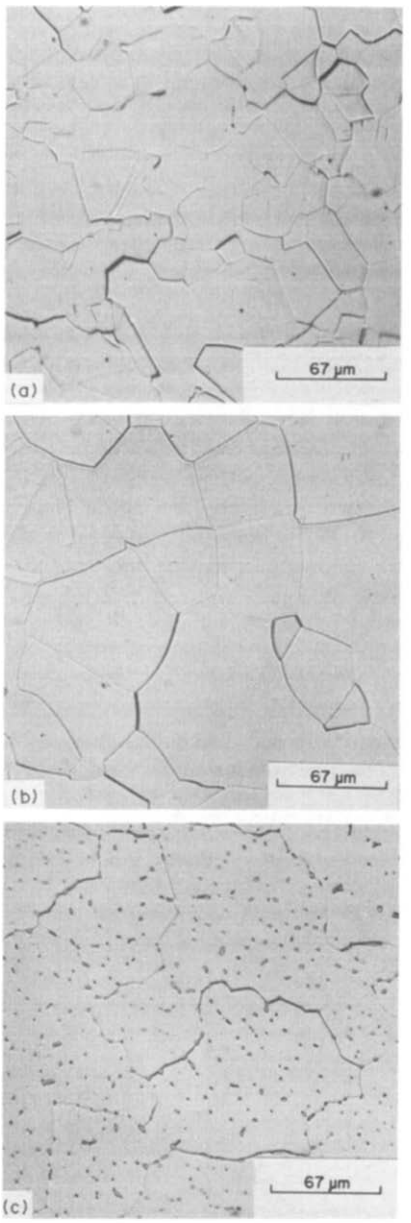

Fig. 1. Optical microstructures of Ni_3Al (24 at.% Al) doped with (a) 0.1, (b) 0.2, and (c) 0.4 wt% B. All specimens were annealed for 30 min at 1000°C.

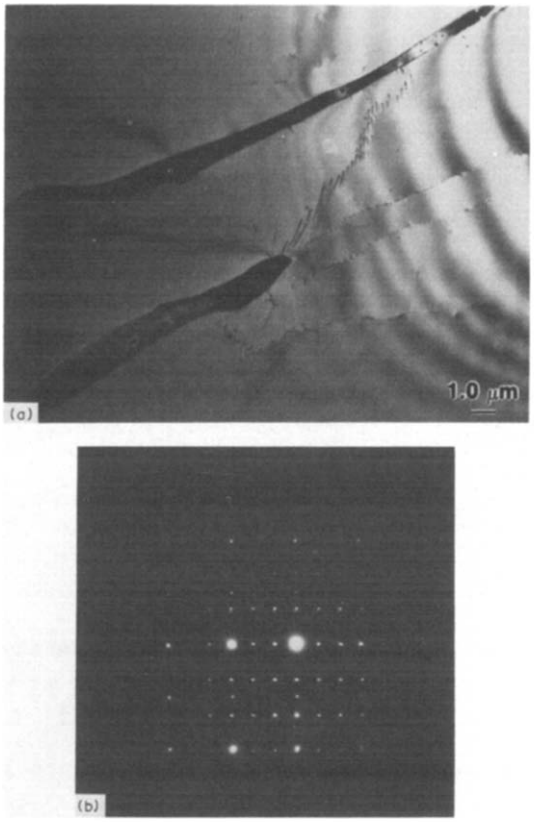

Fig. 2. TEM photographs of Ni_3Al (24 at.% Al) doped with 0.4 wt%B, showing (a) morphology of second-phase particles and (b) their selected-area-diffraction (SAD) pattern. The specimen was annealed for 30 min at 1000°C.

The composition of the particles was determined by both energy dispersive spectroscopy (EDS/TEM) and electron microprobe analysis. The first method gives an aluminum to nickel atom ratio of $14(\pm 2)/86(\pm 2)$ for the particles and 24/76 for the matrix. The second-phase particles are also visible in the electron microprobe image (Fig. 3) obtained using backscattered electrons. The particles are brighter, indicating that they are enriched with heavier elements such as nickel. Microprobe analyses of the particles gives an aluminum to nickel atom ratio of $13.2(\pm 3)/86.8(\pm 3)$. Both analyses indicate the aluminum to nickel atom ratio is consistent with $Ni_{20}Al_3B_6$ for the borides in Ni_3Al doped with 0.4 wt% boron.

Figure 4 shows optical micrographs of 24 to 26 at.% Al aluminides doped with 0.05 and 0.1 wt.% B. All of these aluminides essentially have a single-phase structure. The absence of borides indicates that the solubility of boron in Ni_3Al is not strongly influenced by a variation of aluminum con-

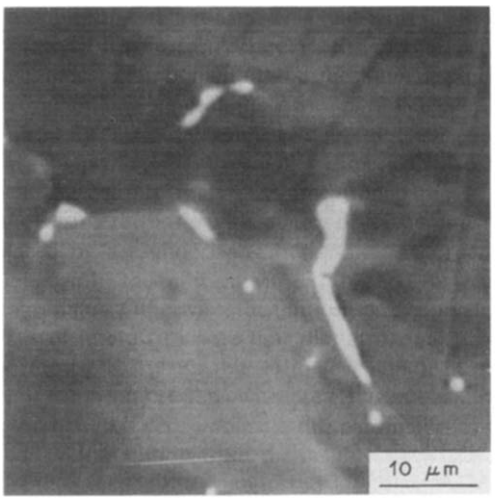

Fig. 3. Electron microprobe image obtained using back-scattered electrons, showing the precipitates in Ni_3Al (24 at.% Al) doped with 0.4 wt% B.

centration in the vicinity of alloy stoichiometry. The few large dots visible in Fig. 4(c) are believed to be voids originated in the cast ingot.

The crystal structure in undoped and B-doped Ni_3Al aluminides was determined by X-ray diffraction. The superlattice lines, which characterize the $L1_2$ ordered crystal structure, were clearly visible, indicating that the boron additions do not affect the long-range ordered crystal structure in Ni_3Al.

Anneal treatment and grain growth

Boron-doped aluminides with 24 at.% Al were annealed for various times (t) at 1000°C, to study their microstructure and grain growth behaviour. The aluminides exhibited significant grain growth during anneals at 1000°C (Fig. 5). TEM micrographs in Fig. 6 reveal no apparent precipitation of borides within grains or along grain boundaries after a long-term anneal of 2.3×10^4 min. Figure 6(b) is a lattice fringe image using (100) superlattice reflections with a spacing of 0.36 nm. The lattice fringe appears to be undistorted, indicating no clusters or precipitates with an estimated diameter >2 nm.

The grain diameter (d) of the annealed samples was measured using a linear intercept method. Figure 7 is a plot of log (d) vs log (t), indicating grain growth behavior of the form.

$$d \propto t^{1/4}. \quad (1)$$

Note that for anneals with longer than 10^4 min the data indicate a slight deviation from the linear relation. This deviation probably results from the grain diameter approaching the sheet thickness (0.76 mm).

Microhardness values of annealed metallographic specimens are plotted vs log(t) in Fig. 8. The specimen annealed for 10 min at 1000°C showed a fine recrystallized grain structure with a hardness of 385 DPH. The hardness decreases continuously to a value of 224 DPH after an anneal of 2.3×10^4 min. This decrease is apparently due to the grain growth at 1000°C.

Tensile properties

Tensile properties of B-doped Ni_3Al were determined as functions of boron concentration, grain size, and alloy stoichiometry. Figure 9 is a plot of room-temperature properties for Ni_3Al (24 at.% Al) doped with various levels of boron. All the specimens were recrystallized for 30 min at 1000°C (grain diameter $\sim 25\,\mu$m). The yield strength increases linearly with boron concentration up to 0.1 wt%. Beyond that level, the strength appears to increase more rapidly with boron concentration and reaches

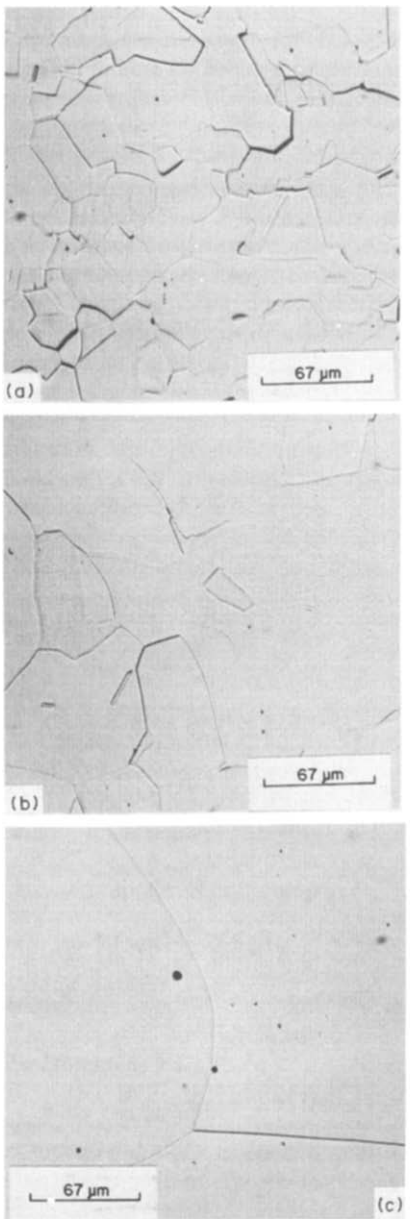

Fig. 4. Optical microstructure of B-doped Ni_3Al aluminides (a) 24 at.% Al and 0.1 wt% B, (b) 25 at.% Al and 0.05 wt% B, and (c) 26 at.% Al and 0.1 wt% B.

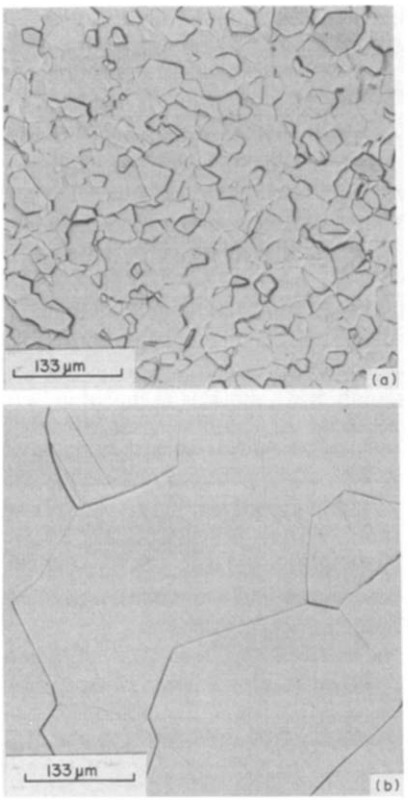

Fig. 5. Grain structures of B-doped Ni_3Al (24 at.% Al) annealed for (a) 10 min and (b) 23,000 min at 1000°C.

486 MPa at 0.2% B. The ultimate tensile strength, however, is not significantly affected by boron concentration.

The ductility of Ni_3Al with at least 0.025 wt% B was determined by tensile tests of sheet specimens, while the ductility for 0, 0.005 and 0.01% B aluminides (which were unfabricable) was estimated from the reduction in thickness during cold fabrication. Undoped Ni_3Al exhibited very little ductility at room temperature. Figure 9 shows a sharp increase in ductility from about 10 to 43.8% as boron levels increase from 0.01 to 0.025 wt% in Ni_3Al. The ductility continues to increase with higher boron levels, reaching 53.8% for the 0.1% B aluminides. With further increases in boron content, the ductility appears to decrease gradually to 39.8% at 0.2% B. Since the 0.4% B aluminide can not be fabricated, its ductility is estimated to be less than 10%.

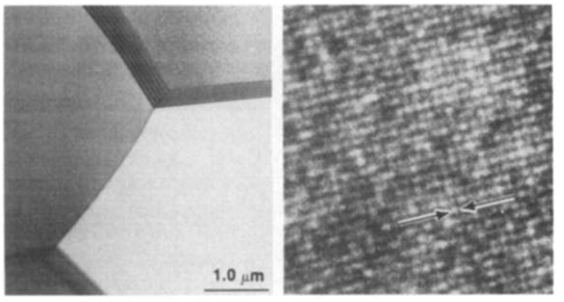

Fig. 6. TEM micrographs of B-doped Ni_3Al (24 at.% Al) sample annealed for 23,000 min at 1000°C. (a) Bright field photo showing no precipitation of borides in grains or along grain boundaries. (b) The lattice fringe image using (100) superlattice reflections with 0.36 nm spacing.

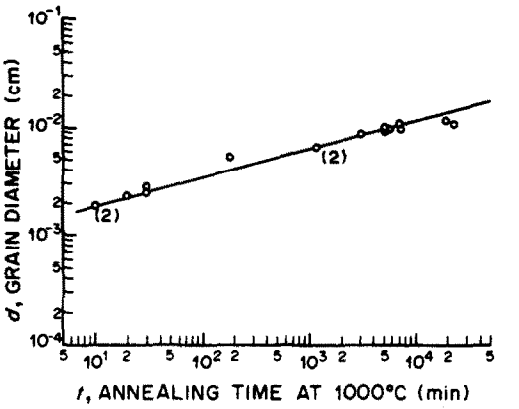

Fig. 7. A plot of log grain diameter, d vs log annealing time, t, for B-doped Ni_3Al (24 at.% Al) annealed at 1000°C, indicating grain growth behaviour.

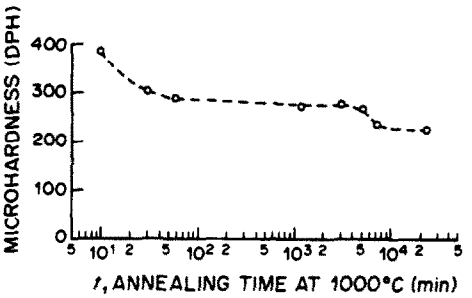

Fig. 8. Plot of microhardness of B-doped Ni_3Al (24 at.% Al) specimens vs logarithm of annealing time at 1000°C.

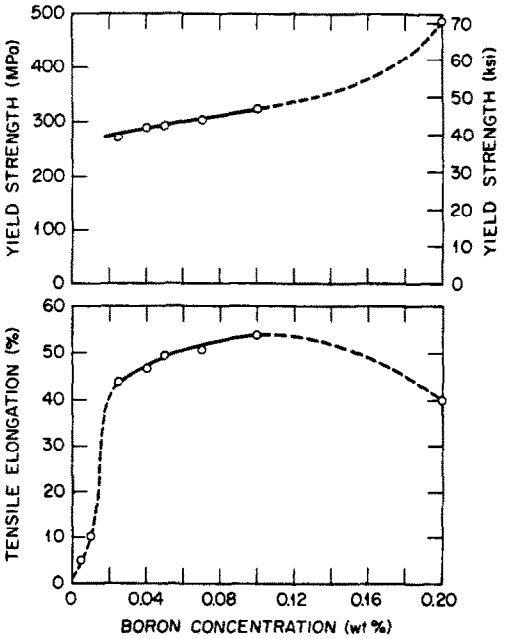

Fig. 9. Plot of room temperature tensile properties as a function of boron concentration for Ni_3Al (24 at.% Al). All specimens were recrystallized for 30 min at 1000°C.

Table 2. Effect of alloy stoichiometry on room temperature tensile properties of Ni_3Al doped with 0.05 wt% B

Alloy No.	Al concentration (at.%)	Elongation (%)	Strength (MPa)	
			Yield	Ultimate
IC-6	24	49.4	290.8	1314.6
IC-42	24.5	37.0	229.7	1161.7
IC-22	24.8	18.5	239.8	652.4
IC-54	25.0	6.0	226.7	354.9
IC-23[a]	25.2	—	—	—
IC-5[a]	26.0	—	—	—

[a]Ingots cracked during fabrication.

Table 2 shows the effect of deviation from stoichiometry on the room-temperature tensile properties of Ni_3Al doped with 0.05 wt% B. The ultimate tensile strength and the total elongation are plotted in Fig. 10 as a function of aluminum concentration. The tensile strength decreases sharply with increasing aluminum concentration above 24 at.%. Since the aluminides, just like other ordered alloys [18], exhibited rapid strain hardening during plastic deformation, the decrease in ultimate tensile strength is essentially due to the sharp drop in ductility with increasing aluminum concentration. In fact, the ductility of B-doped Ni_3Al dropped from 49.4 to 6.0% as the aluminum concentration was increased from 24 to 25 at.%. The tensile properties of the aluminides with >25% Al could not be measured because the ingots cracked during fabrication. These results indicate that a small deviation from stoichiometry strongly influences the ductility and fabricability of B-doped Ni_3Al.

The tensile properties of Ni_3Al (24 at.% Al) doped with 0.1 wt% B were plotted as a function of annealing time at 1000°C in Fig. 11. The yield strength decreases steadily with increased annealing time. Surprisingly, the tensile elongation remains

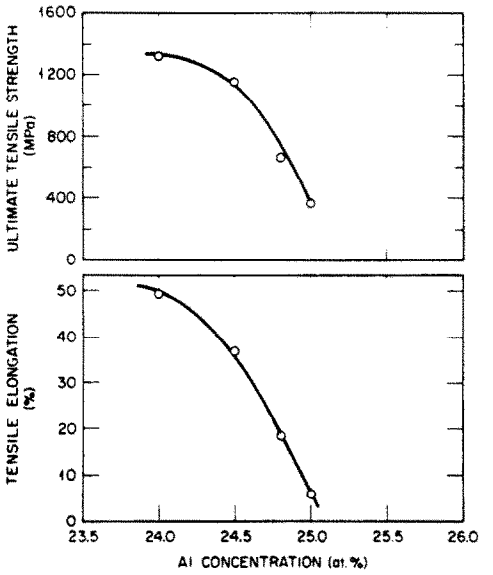

Fig. 10. Plot of room temperature tensile elongation and ultimate tensile strength as a function of aluminum concentration to show the alloy stoichiometry effect.

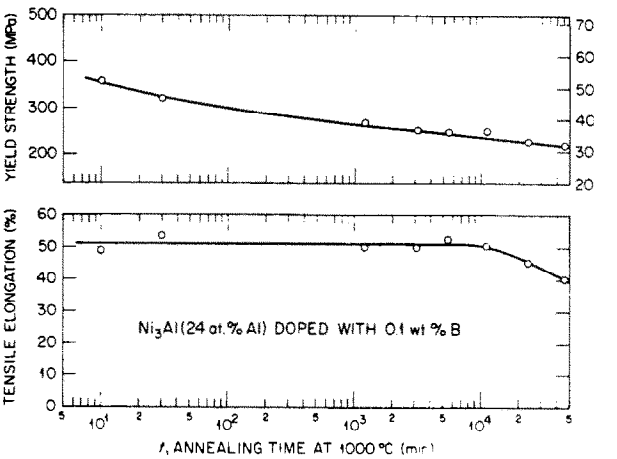

Fig. 11. Plot of tensile properties of Ni_3Al (24 at.% Al) doped with 0.1 wt% B as a function of annealing time at 1000°C.

constant at a level of 50%, independent of annealing time to 10^4 min. With a further increase in annealing time to 5×10^4 min, the aluminide showed only a moderate drop in ductility to 40%.

Fracture behavior

Fracture behavior of Ni_3Al specimens, B-doped or undoped, broken by tensile and bend tests was studied by optical and scanning electron microscopy. Figure 12 shows the brittle grain-boundary fracture observed in undoped Ni_3Al (24 at.% Al). The grain-boundary facets are smooth and free from any deformation marks, indicating the brittleness of the boundaries. Occasionally, foreign inclusions/voids were observed on certain grain boundaries. The effect of alloy stoichiometry on fracture behavior is shown in Fig. 13 for Ni_3Al aluminides doped with 0.05 wt%. B. The B-doped aluminide with 24% Al exhibited almost completely transgranular fracture

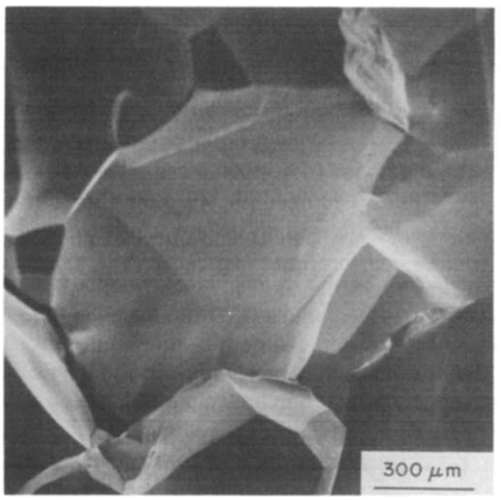

Fig. 12. SEM fractograph of undoped Ni_3Al (24 at.% Al), showing brittle grain-boundary fracture at room temperature.

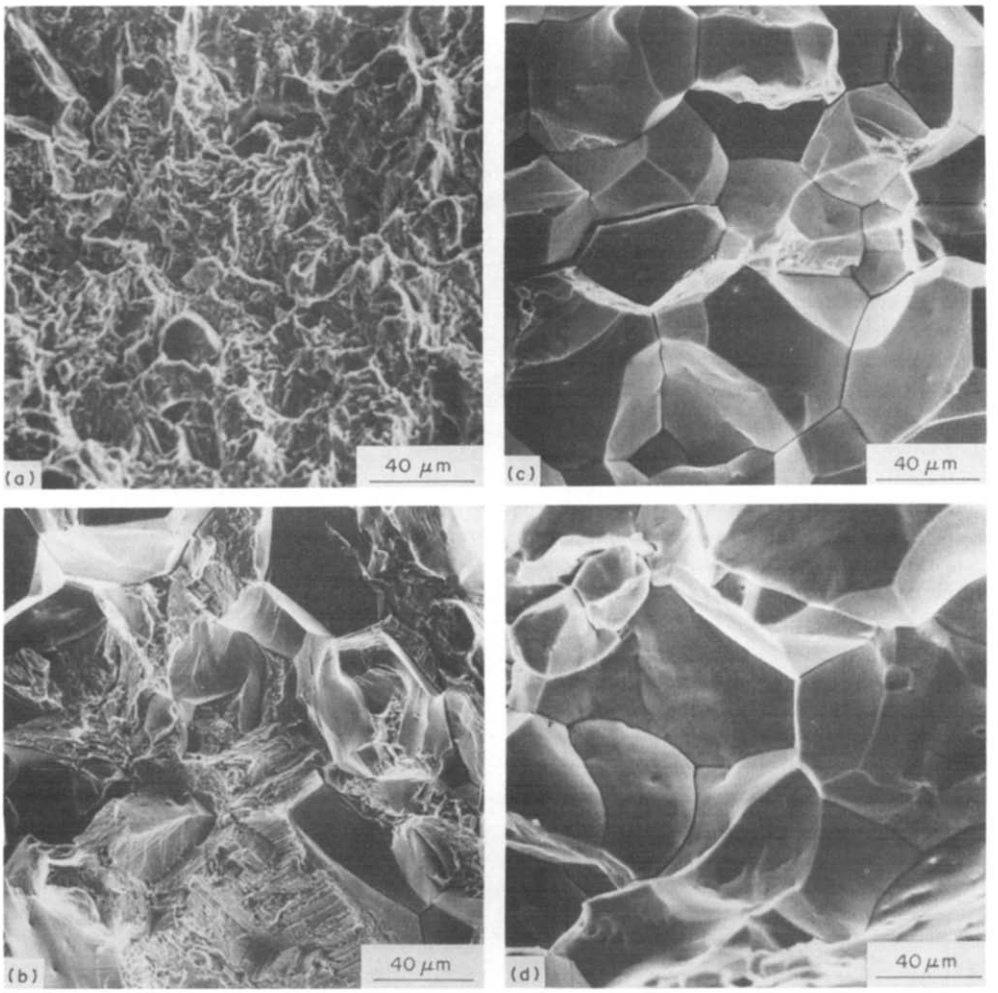

Fig. 13. SEM fractographs of Ni_3Al doped with 0.05 wt%B, showing the effect of alloy stoichiometry on fracture behavior at room temperature (a) 24 at.% Al, tensile fractured, (b) 24.5 at.% Al, tensile fractured, (c) 24.8 at.% Al, tensile fractured, and (d) 26 at.% Al, fractured by bending.

[Fig. 13(a)]. Microscopically the fracture surface of the specimen is slanted at about 45° to the tensile axis, corresponding approximately to the plane of maximum shear stress. With an increase in aluminum concentration to 24.5%, the aluminide showed a mixed mode of intergranular and transgranular fracture [Fig. 13(b)], with secondary cracks and slip marks visible on grain boundaries. With a further increase in aluminum content, the aluminides fractured essentially intergranularly [Fig. 13(c) and (d)]. Note that the 24.8% Al aluminide had a tensile ductility of 18.5%, even though it fractured intergranularly.

Figures 14–16 show the effect of heat treatment on fracture behavior of Ni_3Al (24 at.% Al) doped with 0.1 wt% B. The specimens annealed for 30 min exhibited transgranular fracture with a ductile dimple-type fracture mode [Fig. 14(a) and (b)]. Slip traces and transgranular cracks are clearly visible on external surfaces of the deformed specimens [Fig. 14(c)]. With the increase in annealing time to 5×10^4 min, there is no change in the basic fracture mode (i.e. transgranular); however, some additional fracture features are observed as shown in Figs 15 and 16. The fracture surface of the tensile specimen annealed for 2.3×10^4 min at 1000°C contains jagged areas of well-defined facets, possibly corresponding to crystallographic planes (Fig. 15). Also, isolated grain-boundary facets with extensive slip marks were observed for the specimen annealed for 4.6×10^4 min (Fig. 16).

Auger electron spectroscopy

Auger analyses from intergranular fracture of undoped aluminides generally indicated slight concentrations of sulfur (< 1 at.%) with little other evidence of impurity segregation as indicated in curve (a) of Fig. 17. Intergranular regions on fractured B-doped specimens all exhibited significant boron enrichment at the grain boundaries as indicated in curves (b) and (d) of Fig. 17. Although there were small variations in sulfur intensity from specimen to specimen, and even from point to point on a given fracture surface,

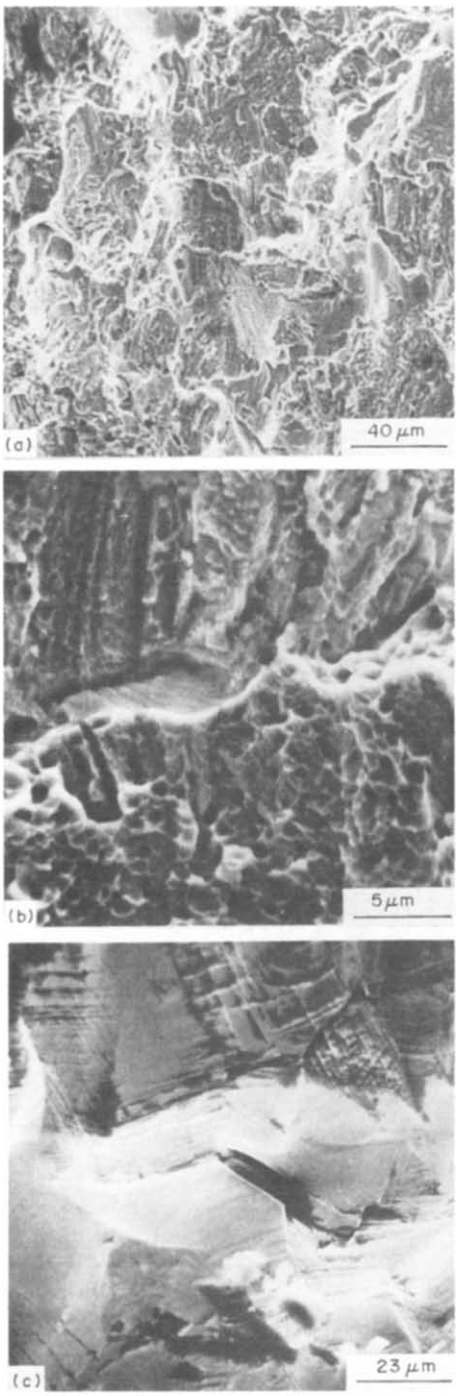

Fig. 14. Room temperature fracture behavior of Ni_3Al (24 at.%Al) doped with 0.1 wt% B. (a) SEM fractograph showing transgranular fracture, (b) high-magnification view of (b) showing dimple structures, and (c) slip marks and a transgranular crack on specimen surface.

there was no observed correlation with boron additions or aluminum content.

There was a correlation, however, between the intensity of boron segregation and aluminum content. For the purpose of comparison, we have used the ratio of peak-to-peak intensities for the 180 eV B and 102 eV Ni Auger peaks (henceforth we call this ratio PHR (B/Ni)]† as a measure of the boron concentration at the fracture surface. An estimate of the atomic ratio can be obtained from PHR values, using relative elemental sensitivities from published standard spectra of pure elements [19]. The sensitivity of the 180 eV boron peak is approx. 5.5 times that for 102 eV Ni, indicating that PHR(B/Ni) can be divided by 5.5 to estimate B/Ni atom ratios.

Comparison of curves (b) and (d) in Fig. 17 shows PHR(B/Ni) decreases from ~1.03 for Ni–24 at.% Al–0.05 wt% B to ~0.54 for Ni–25 at.% Al–0.05 wt% B. Mean values of PHR (B/Ni) are plotted vs aluminum concentrations in Fig. 18 for aluminides doped with 0.05 wt% B. Figure 18 also shows the ratio of the 1396 eV Al peak to the 848 eV Ni peak, PHR(Al/Ni), plotted versus aluminum content in these aluminides. The plot shows a general trend of increasing the grain-boundary

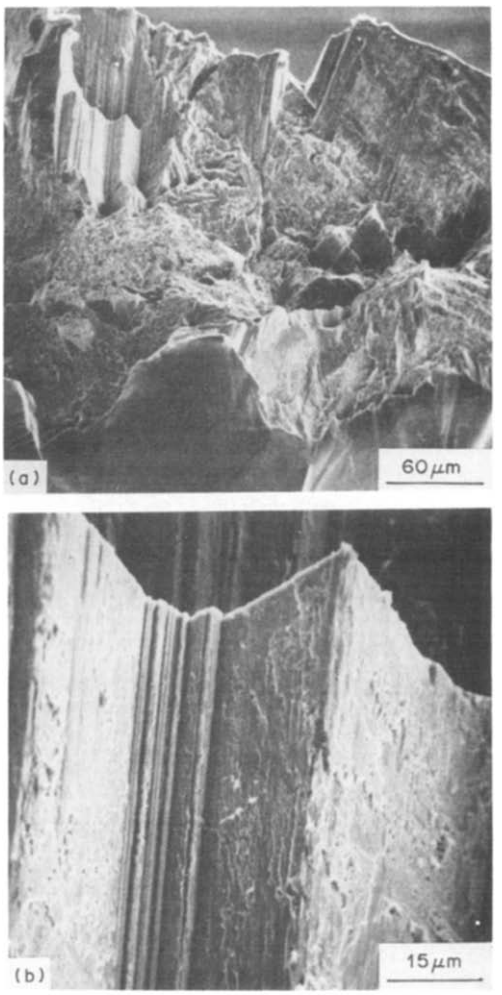

Fig. 15. SEM fractographs of 0.1 wt% B–Ni_3Al (24 at.% Al) annealed for 23,000 min at 1000 C and tensile fractured at room temperature (a) low magnification view showing transgranular fracture, and (b) high magnification view showing jagged fracture facets.

†PHR = peak-height-ratio.

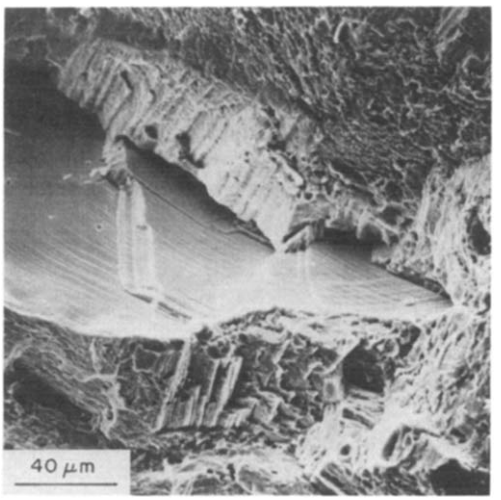

Fig. 16. SEM fractograph showing a grain-boundary facet surrounded by transgranular fracture regions.

PHR(Al/Ni) with the bulk aluminum concentration. The aluminide containing 24 at.% Al exhibited significant portions of transgranular fracture, which yielded PHR(Al/Ni) $\simeq$ 0.155.

Sputter etching the fracture surfaces for 2 min removed essentially all of the boron and sulfur from the intergranular regions [Fig. 17(c)]. Sputtering was also noted to reduce PHR(Al/Ni) values, however this effect was observed on transgranular as well as intergranular regions of aluminides containing 24 and 24.5 at.% Al. This latter observation suggests that aluminum may be preferentially removed during the sputter etching process, complicating the interpretation of sputtering results for the high aluminum alloys.

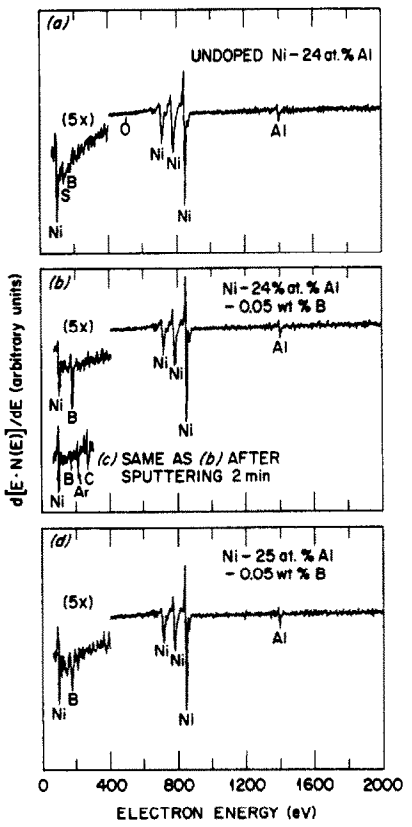

Fig. 17. Auger spectra obtained from intergranular area or fracture surfaces of undoped and B-doped Ni_3Al specimens. (a) Undoped Ni–24 at.% Al. (b) Ni–24 at.% Al–0.5 wt% B. (c) Same as (b) after sputtered for 2 min. (d) Ni–25 at.% Al–0.05 wt% B.

Auger spectra from specimens having aluminum contents greater than 24.5 at.% occasionally exhibited small sulfur-rich spots on the intergranular fracture surfaces. Figure 19 shows Auger spectra [(a)–(c)], secondary electron images [(d) and (e)], and an elemental sulfur map (f), which describe such a region in a Ni–25.2 at. % Al–0.05 wt% B specimen. Curve (a) shows a typical Auger spectrum for the smooth grain boundary region at point A in image (d). Curve (b) shows a partial spectrum from the feature at point B in image (e). Comparison of curves (a) and (b) clearly indicates that point B is highly enriched in sulfur, and has little if any boron. Mapping the intensity of the sulfur peak over the same field of view shown in (e) yielded the sulfur map (f). Sputter etching for 2 min and re-analysis of point B (see curve c) indicated that the sulfur-rich region was only a few atom layers thick. Because of its appearance in Fig. 19(e), and the thinness of the sulfur-rich region, we believe that the feature at point B is a grain-boundary cavity most probably retained from the casting process. These results indicate that sulfur segregates much more strongly to free surfaces than to grain boundaries, while the reverse appears to be true for boron.

Analysis of B-doped and undoped specimens containing 26 at.% Al revealed spherical Al-rich pre-

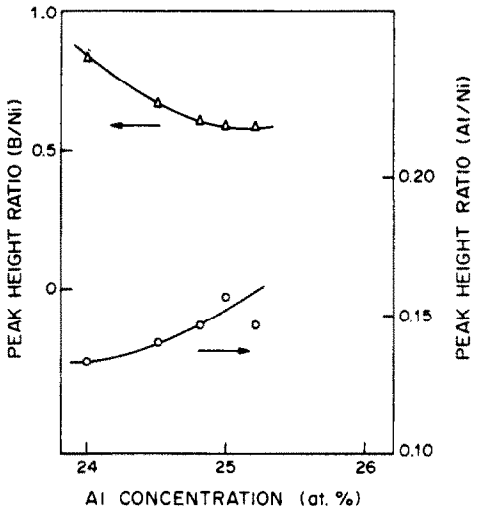

Fig. 18. Correlation of PHR(B, 180 eV/Ni, 102 eV) and PHR(Al, 1396 eV/Ni, 848 eV) with aluminum concentration. The peak-height-ratios were obtained from intergranular portions of fracture surfaces of Ni_3Al–0.05 wt% B.

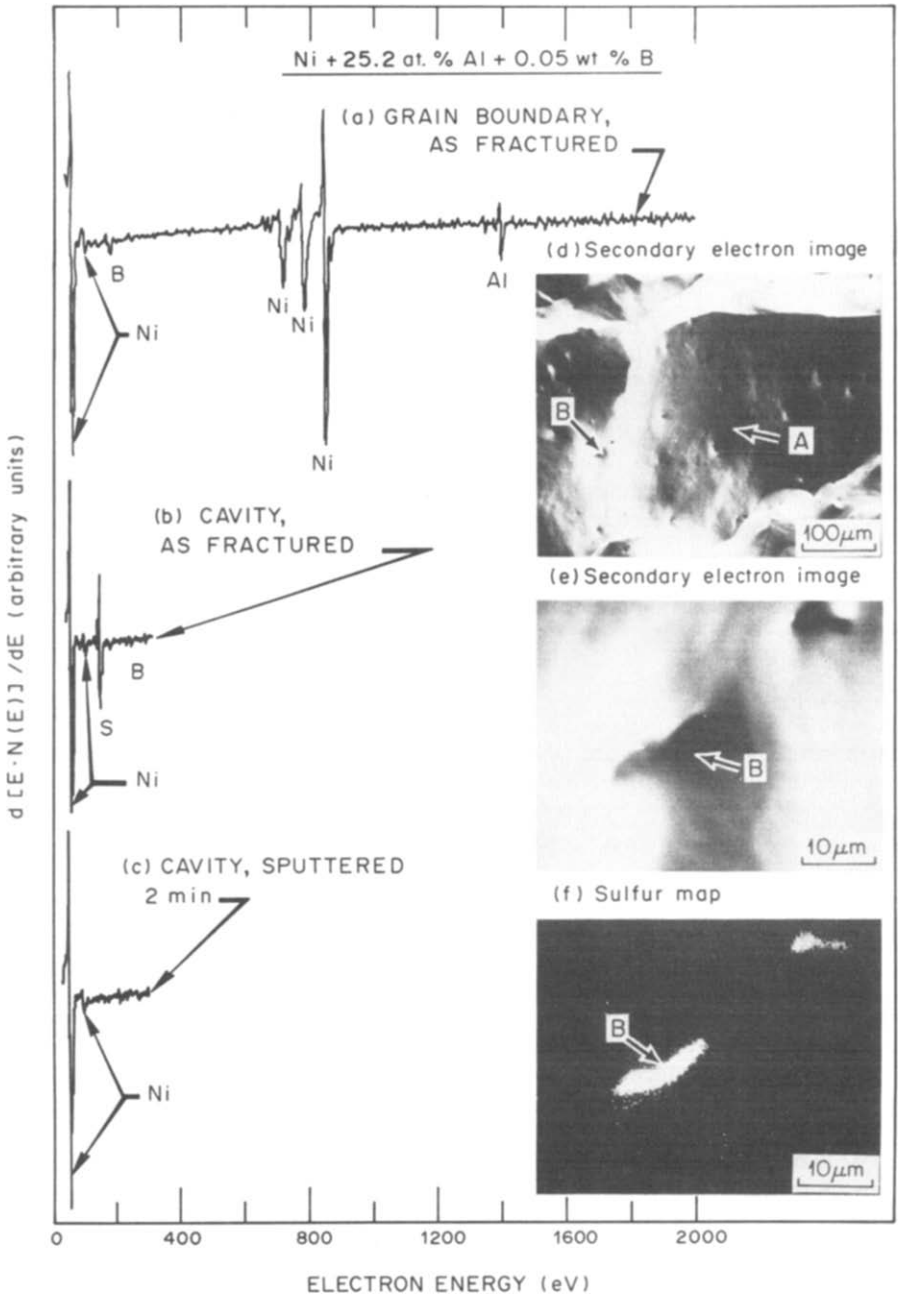

Fig. 19. Auger spectra [(a)–(c)], secondary electron images [(d) and (e)], and a sulfur elemental map (f), describing a region on a fracture surface of Ni–25.2 at.% Al–0.05 wt% B. The Auger spectrum in (a) was obtained from the smooth grain-boundary region at point "A" in image (d), and the partial spectrum was from the feature at point "B" in image (e).

cipitates on the grain boundaries of the cast and homogenized aluminides. Auger analysis on the precipitates indicated PHR(Al/Ni) in the range 0.26–0.29 as opposed to 0.15–0.18 for grain boundaries. The precipitates did not appear to be enriched in sulfur (or in the case of B-doped specimens, in boron), indicating that they are probably NiAl particles.

DISCUSSION

To understand the beneficial effect of boron, we need, first of all, to identify the potential source(s) of grain-boundary brittleness in Ni_3Al. The grain boundaries in Ni_3Al could be intrinsically brittle due to poor cohesion, or extrinsically brittle due to

segregation of trace impurities. The impurity levels are quite low in undoped Ni_3Al (IC-2) as indicated in Table 1. Auger analysis reveals that its grain boundaries are quite clean and free from oxygen and carbon. A small amount of sulfur (a trace impurity in Ni_3Al), less than 1 at.%, was present at the grain boundaries; however, the level seems to be too low to cause any severe embrittlement. We also prepared high-purity Ni_3Al using 99.999% aluminum and nickel metals. Preliminary results [20] show that the aluminide remains brittle and exhibits brittle intergranular fracture without sulfur present at the grain boundaries. Aoki and Izumi [13] had found that the ductility and fabrication could not be improved by lowering impurities in Ni_3Al. Recently, Koch *et al.* [21] observed that polycrystalline Ni_3Al foils remain brittle when prepared by rapid solidification which was used to suppress impurity segregation. All these results suggest that the intrinsic weakness (i.e. poor cohesion) is the primary source of the grain-boundary brittleness in Ni_3Al. Of course, the boundaries can be further embrittled by segregation of significant amounts of harmful impurities, such as sulfur, in impure Ni_3Al materials. The intrinsic nature of grain-boundary brittleness has been observed in other face-centered cubic (f.c.c.) metals and alloys. For instance, recent studies [22–24] of precious metal alloys indicated that the grain boundaries in iridium alloys are intrinsically brittle without impurities segregated on them.

Our studies have demonstrated that the ductility and fabricability of Ni_3Al containing 24 at.% Al can be dramatically improved by boron additions. The boron dopant added to Ni_3Al is retained in solid solution until exceeding its solubility limit. The precipitation of second-phase particles was observed in the alloy doped with 0.4 wt% B. Both TEM and electron microprobe analyses indicate that the particles have an fcc tau phase structure with a composition of $Ni_{20}Al_3B_6$. This is consistent with the tau phase observed in the Ni–Al–B system by Stadelmaier *et al.* [25–27]. The solubility limit of boron in Ni_3Al is estimated to be 0.3 ± 0.05 wt%, which appears not to be affected by alloy stoichiometry.

Boron, even within its solubility limit, does not distribute uniformly in Ni_3Al. Auger studies reveal that boron has a strong tendency to segregate to grain boundaries, particularly Ni_3Al containing 24 at.% Al (Fig. 17). Based on the peak-height-ratio of boron to nickel, the boron concentration at the boundaries is estimated to be about 10 at.% in the 24% Al aluminide. The boron peak totally disappears after sputtering 3–4 atomic layers from the boundaries, indicating no formation of a boron-containing second phase. Analyses of a cavity surface (Fig. 19) indicated little if any tendency for boron segregation, and extensive sulfur segregation, to free surfaces, in agreement with surface segregation studies by Yalisov and Graham [28]. Sulfur, an impurity in Ni_3Al, is present at the grain boundaries in the same level (< 1 at.%) in both undoped and B-doped Ni_3Al. Thus, the presence of boron apparently does not affect the sulfur segregation or scavenge sulfur from the grain-boundary region. Since the 24% Al aluminide exhibited completely transgranular fracture, the presence of a sufficient amount of boron (~ 10 at.%) at the grain boundaries must reduce the tendency towards intergranular fracture, thereby dramatically improving the overall ductility and fabricability of the aluminide.

The effects of segregating solutes on grain-boundary cohesion have been the subject of numerous experimental and theoretical investigations; however, the vast majority of such inquiries have dealt with embrittling solutes [29] and relatively few address beneficial effects of segregating solutes [22, 30]. Recently Messmer and Briant [31, 32] proposed an electronic model to explain the effects of alloying elements on grain-boundary cohesion in metals. According to their model, the embrittling elements, such as sulfur, are those which are electronegative with respect to base metals, such as nickel and iron. These elements draw charge from the neighboring metal atoms onto themselves; consequently less charge is available to participate in the metal–metal bonds which are weakened. The beneficial elements, such as boron, are those which are less electronegative with respect to the base metals. These elements do not draw charge off the metal atoms and thus do not weaken the metal–metal bonds. Furthermore, these elements share electrons with the metal atoms (i.e. formation homopolar bonds) and thus enhance bonding in the grain boundary. Messmer and Briant verified their model to a certain extent, using quantum-mechanical cluster calculations. Based on this model, boron, which tends to segregate strongly in Ni_3Al, enhances bonding between nickel atoms and results in improvement of grain-boundary cohesion and reduction of the tendency toward brittle intergranular fracture.

Early thermodynamic treatments of segregation effects on grain-boundary cohesion evolved from the Griffith approach to brittle elastic fracture [33] where Griffith's $2\gamma_s$ term (γ_s = surface energy of the newly created fracture surface) was replaced by

$$\phi = 2\gamma_s - \gamma_b \qquad (2)$$

where γ_b is the energy of the grain boundary, and ϕ is the ideal grain-boundary cohesive energy.† Segre-

†As with the original Griffith approach, and any purely thermodynamic approach, we are considering here purely elastic fracture of mode II or III type. Metals, of course, rarely exhibit purely elastic fracture, since some plastic flow nearly always accompanies the crack tip stresses necessary for decohesion. It has been argued, however, that ϕ can play a major role in intergranular fracture even when ϕ is much smaller than the plastic work associated with fracture. The so-called "valve effect" of ϕ was introduced by McLean [34] and refined by subsequent investigators [35, 36].

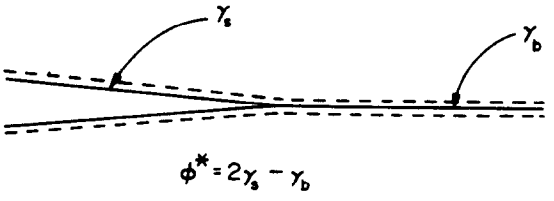

Fig. 20. Grain-boundary cohesive energy, ϕ^*, required for propagation of a crack along a solute-segregated boundary.

gating solutes were postulated to exert their influence on ϕ by affecting γ_s and γ_b (Fig. 20). The equilibrium relationship between any interfacial energy, γ, and the chemical potential of a segregating solute, μ_N, is described by the Gibbs adsorption equation, given in equation (3a) for the case of a binary solid solution M–N at constant temperature.

$$d\gamma = -\left[\Gamma_N - \left(\frac{X_N}{1-X_N}\right)\Gamma_M\right] d\mu_N \quad (3a)$$

$$= -\Gamma\, d\mu_N \quad (3b)$$

The terms Γ_M and Γ_N in equation (3a) are interfacial excesses of the solvent and solute species, respectively. Although these quantities depend upon the exact location of a hypothetical interfacial plane, the total quantity in brackets [denoted as Γ in equation (3b)] is independent of the frame of reference [37]. Additions of strongly segregating solutes (i.e. those for which $\Gamma > 0$) will cause $d\gamma$ to be negative and lead to reductions in interfacial energies. This effect is, in fact, observed in measurements of γ_s and γ_b using zero creep techniques at temperatures $\sim 0.9\, T_m$. Asaro [38] has reported calculations on the Fe–P system using γ_b and γ_s measurements by Hondros [39], showing that phosphorus additions (which are known to segregate to, and embrittle grain boundaries) lower ϕ if the grain-boundary crack propagates sufficiently slowly, and the temperature is sufficiently high to maintain equilibrium at the advancing crack tip.

In the present situation, however, we are concerned with rapid grain boundary crack propagation at relatively low temperatures. Several investigators have noted that the fracture surface created during such a process will not generally have a level of solute segregation that is in equilibrium with the adjacent grains. These surfaces will, instead, inherit an adsorption level that is one-half that for the grain boundary. The surface energy of such a non-equilibrium surface, γ_s^*, will not be described directly by equation (3), and will result in a cohesive energy, ϕ^* that will not generally equal that for fracture under equilibrium conditions, ϕ. Rice was apparently the first to treat this aspect of rapid fracture in a rigorous fashion [40], and several investigators have subsequently clarified the significance and implications of his treatment† [38, 41, 42]. Equation (4) shows the differential relationship between ϕ^* and Γ^b from Rice's original work (equation (10) in Ref. [40]).

$$\frac{d\phi^*}{d\Gamma^b} = \mu_N^s(\Gamma^b/2) - \mu_N^b(\Gamma^b). \quad (4)$$

In equation (4), the function μ_N^b describes the solute chemical potential as a function of equilibrium grain-boundary excess, Γ^b (see solid curves in Fig. 21). The function μ_N^s describes the same solute chemical potential as a function of equilibrium surface excess, Γ^s; and is evaluated at $\Gamma^s = \Gamma^b/2$ in equation (4) (dashed curves in Fig. 21). This means that $\mu_N^s(\Gamma^b/2)$ is the solute chemical potential that would result in an equilibrium surface excess equal to half the grain-boundary excess for the grain boundary that is actually undergoing fracture. The relationship between $\mu_N^b(\Gamma^b)$ and $\mu_M^s(\Gamma^b/2)$ is illustrated schematically in Fig. 21 for two qualitatively different types of solute segregation behavior.

Normally trace element segregation to free surfaces is observed to be much stronger than to grain boundaries (i.e. $\Gamma^s > \Gamma^b$). This situation is depicted schematically in Fig. 21(a), which corresponds qualitatively to the sulfur segregation observed in the present study. For a specific solute concentration and corresponding chemical potential, $\mu_b = \mu_N^b(\Gamma^{b'})$, the grain boundaries are assumed to be equilibrated having an excess $\Gamma^b = \Gamma^{b'}$. The solute excess on a rapidly created intergranular fracture surface, $(\Gamma^{b'}/2)$, would be much less than the equilibrium level, $\Gamma^{s'}$, corresponding to the actual chemical potential, $\mu_M^s(\Gamma^{s'})$. [Note that for equilibrium separation $\mu_N = \mu_M^b(\Gamma^{b'}) = \mu_M^s(\Gamma^{s'})$]. The "surface" chemical potential, $\mu_M^s(\Gamma^{b'}/2)$, is correspondingly less than $\mu_M^b(\Gamma^{b'})$ yielding a negative value of $d\phi^*/d\Gamma^b$ and indicating a loss in cohesion due to segregation.

In contrast to sulfur, boron has been observed to segregate much more strongly to grain boundaries than to free (cavity) surfaces. The curves in Fig. 21(b) correspond to such a situation, where $\Gamma^b \gg \Gamma^s$. Following an argument similar to the one for Fig. 21(a), we conclude that $\mu_M^s(\Gamma^{b'}/2) > \mu_M^b(\Gamma^{b'})$; and hence by equation (4), ϕ^* should increase with solute additions.

We should note that $\Gamma^b > \Gamma^s$ is a necessary but not sufficient condition for increasing ϕ^*, since the right side of equation (4) can remain negative if the curve for Γ^s is only slightly below the one for Γ^b in Fig. 21(b). If we make the simplifying assumptions that Γ^b and Γ^s are linearly proportional to solute atom fraction, and that the solute obeys Henry's law, it is straightforward to show what $\Gamma^b > 2\Gamma^s$ is the condition for the solute segregation to increase ϕ^*. These

†We note here that grain boundaries will not generally be in equilibrium with adjacent grains either, since we are often considering fracture at temperatures on the order of $0.2\, T_m$ where equilibration can be very slow. It appears that such deviations from equilibrium would also be treatable using Rice's approach; however, this aspect of the problem does not appear to have been considered in any detail.

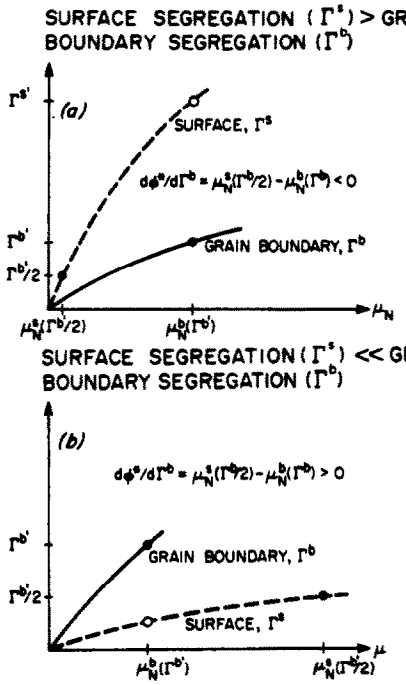

Fig. 21. A schematic diagram showing the effect of solute segregation on the solute chemical potential of free (cavity) surfaces, μ_N^s, and grain boundaries, μ_N^b for two types of solutes. (a) The solute has a strong tendency to segregate to grain boundaries but not to free surfaces, and (b) the solute tends to segregate more strongly to free surfaces than to grain boundaries.

assumptions should be substantially valid for any system at extreme dilution.

In terms of PHR values from AES spectra, to a first approximation, the ratio $\Gamma^s/\Gamma^b = (1/2)(PHR^s/PHR^b)$. The factor of (1/2) arises from the fact that only one-half of the grain-boundary solute content is measured in the Auger spectrum, while all of the surface solute is measured. Other factors, such as differences between solute distributions at free surfaces and grain boundaries will also influence the relationship between Γ^s/Γ^b and PHR^s/PHR^b, but such second order considerations are probably not important for the largely qualitative discussions in this paper. It is sufficient to note that for the case of extreme dilution, the condition that $\Gamma^b > /2\Gamma^s$ corresponds to $PHR^b > PHR^s$, a condition that is clearly satisfied by PHR(B/Ni) values from Fig. 19. It follows then that boron segregation to grain boundaries should increase ϕ^* in qualitative agreement with our experimental observations.

Clearly, if Rice's treatment of segregation effects on grain-boundary cohesion is generally applicable, comparison of surface and grain-boundary segregation using established microanalytical techniques could be very useful in screening candidate microalloying constituents. In systems for which control or prevention of grain-boundary fracture is a major consideration, one would look for elements that segregate much more strongly to grain boundaries than to free surface.

The most interesting finding in this study is that the aluminum concentration around alloy stoichiometry strongly influences the ductility and fracture behavior of B-doped Ni_3Al. The boron dopants are most effective in improving the ductility and suppressing the brittle grain-boundary fracture in the 24% Al aluminide. However, its ductilization effect becomes less prominant in Ni_3Al with higher aluminum concentrations. As shown in Figs 10 and 12, the tensile ductility decreases and the propensity for grain-boundary fracture increases with the increase in aluminum approaching its stoichiometric composition, i.e. 25 at.%Al. The aluminide with 24.8% Al exhibited predominantly intergranular fracture, even though it had 18.5% elongation at room temperature. The effect of stoichiometry can be partially understood based on its effect on boron segregation. The level of boron segregated to the grain boundaries decreases with the increase in aluminum concentration in Ni_3Al (Fig. 18). That is, the boron becomes less effective in ductilization Ni_3Al when there is less than a critical amount of boron ($\sim$10 at.% B) present at the grain boundaries. Ongoing research on these aluminides will include surface segregation studies, to better characterize boron segregation to free surfaces, and any effects of aluminum content on that segregation.

The increase in the bulk concentration of aluminum also results in a higher level of aluminum at the grain boundaries in Ni_3Al, as indicated in Fig. 18.The enrichment of grain-boundary aluminum may reduce the electronic interaction between nickel and boron atoms at the boundaries, thereby lowering the ductilization effect of boron. Alloy stoichiometry is also known to affect the defect structures (such as interstitials, vacancies, and anti-structure defects in ordered intermetallic compounds [43–46]. Further study is required to characterize the defect structures, particularly near grain boundaries, in hyper- and hypo-stoichiometric Ni_3Al.

Recently, Noguchi *et al.* [47] have observed that deviations from stoichiometry strongly influence the positive temperature dependence of yield strength of Ni_3Al and Ni_3Ga. Their yield strength showed a more pronounced increase with increasing test temperature for the alloys with higher aluminum and germanium concentrations.

The annealing treatment at 1000°C resulted in a significant increase in grain size (Fig. 7) and a decrease in yield strength (Fig. 11) of B-doped Ni_3Al. To analyze the grain size effect, the yield strength, σ_y, is plotted as a function of $d^{-1/2}$ in Fig. 22, where d is the grain diameter. The plot in Fig. 22 shows a linear relation held well between σ_y and $d^{-1/2}$, indicating that the yield stress of the B-doped Ni_3Al obeys the Hall–Petch relation [48, 49].

$$\sigma_y = \sigma_{0,y} + k_y d^{-1/2} \tag{5}$$

where $\sigma_{0,y}$ and k_y are the Hall–Petch material constants. Aoki and Izume [13] reported a yield stress of

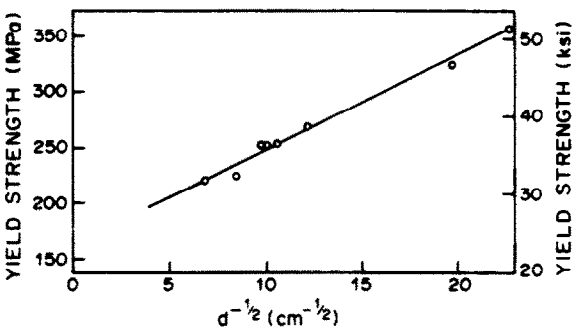

Fig. 22. The Hall–Petch plot of yield stress of B-doped Ni_3Al (24 at.% Al) as a function of $d^{-1/2}$ (d = grain diameter).

200 MPa (29 ksi) for B-doped Ni_3Al with a grain diameter of 1×10^{-2} cm. Their yield stress is considerably lower than the present results (as compared on the same grain size), and thus it does not fit the linear relation in Fig. 22.

The Hall–Petch constants, which can be determined from the intercept and slope of the line in Fig. 22, are measured to be 163 MPa for $\sigma_{0,y}$ and 8.2 MPa $cm^{1/2}$ for k_y. The constant k_y is a measure of the grain-boundary's resistance to the transmission of slip from one grain to the next. In terms of a dislocation model [49, 50], k_y is related to the stress concentration required to operate dislocation sources at or near grain boundaries in unyielded grains. The k_y value for B-doped Ni_3Al is comparable to that of other $L1_2$ ordered alloys such as Zr_3Al [51] (= 7.6 MPa $cm^{1/2}$) Ni_3Mn [52] (= 10.8), Cu_3Au [58] (= 5.0), and Ni_3Fe [54] (= 12.4). If the frictional stress of dislocations on their slip planes $\sigma_{0,y}$, is divided by an average orientation factor [55] of 2.85 to relate the polycrystal yield stress to the single crystal shear stress [56], a resolved shear stress value of 57 MPa is obtained for B-doped Ni_3Al. This value compares reasonably well with the critical resolved shear stress (CRSS) values for Ni_3Al single crystals, reported [57] to be about 40 MPa on {111} planes.

The fracture mode and tensile ductility of B-doped Ni_3Al (24 at.% Al) are not affected by annealing up to 10^4 min at 1000°C. Further anneals cause only a moderate decrease in ductility, but no change in fracture mode, i.e. transgranular fracture persists.

Examination of fracture surfaces suggests that the limited loss in ductility may be related to a high stress concentration at grain boundaries in coarse-grained Ni_3Al. In these specimens the stress concentration may be high enough to induce microcracks within grains (Fig. 15) or along grain boundaries (Fig. 16). The propagation of these cracks transgranularly leads to a premature fracture of the long-term annealed specimens. The jagged fracture surface with {100} facets were observed [58] in single crystals of Ni_3Ge, another $L1_2$ ordered alloy which had less than 10% ductility at room temperature.

The ductility and fabrication behavior of B-doped Ni_3Al with less than 0.025 wt%B is so low that it cannot be satisfactorily fabricated into sheets because of severe grain-boundary cracking. On the other hand, sheet fabricability becomes increasingly difficult for Ni_3Al doped with more than 0.1 wt%B. The aluminides doped with 0.025–0.2% B all had excellent tensile elongation (>40%) at room temperature, even though a ductility maximum appears to be at 0.1% B. In view of these results, the optimum level of boron in Ni_3Al (24 at.% Al) should be 0.06 ± 0.02) wt%.

SUMMARY AND CONCLUSIONS

1. Ni_3Al alloys containing 24–26 at.% Al were doped with a variety of boron contents (up to 0.4 wt% or 1.9 at.%) to study the effects of boron additions on grain-boundary chemistry and tensile properties.

2. The solubility limit of boron in Ni_3Al is roughly equal to $0.3 + 0.05$ wt%; beyond that level, second-phase particles with a composition of $Ni_{20}Al_3B_6$ were observed.

3. Boron-doped Ni_3Al with 24% Al was readily fabricated into sheet by repeatedly cold rolling and annealing. Sheet fabrication became increasingly difficult as the aluminum content was increased; aluminides with >25% Al could not be successfully cold fabricated into sheets.

4. The room temperature ductility of Ni_3Al with 24 at.% Al increases sharply with boron concentration and reaches a broad maximum of 53.8% for the 0.1 wt% B aluminide. With a further increase in boron, the ductility exhibits a modest decrease to 39.8% at 0.2% B (Fig. 9).

5. Room-temperature ductility and fracture behaviour of boron-doped Ni_3Al are critically dependent on deviation from alloy stoichiometry. As the aluminum content of B-doped Ni_3Al is decreased below 25 at.%, the ductility increases dramatically (Fig. 10). Correspondingly, there is a sharp change in fracture mode from intergranular, through a mixed mode, to transgranular as the aluminum content decreases from 25 to 24 at.% (Fig. 13).

6. AES studies of freshly fractured surfaces of B-doped Ni_3Al samples reveal that the aluminum content has no observable effects on carbon, oxygen, and sulfur segregation. Instead, the intensity of boron segregated to grain boundaries increases, and the amount of grain-boundary aluminum decreases significantly, with decreasing bulk aluminum concentration (Fig. 18). These results indicate that alloy stoichiometry strongly influences grain-boundary chemistry, which, in turn, affects the grain-boundary cohesion and overall ductility of nickel aluminides.

7. Boron exhibits an unusual segregation behavior in Ni_3Al. That is, boron has a strong tendency to segregate to the grain boundaries but not to cavity (or free) surfaces (Fig. 19). On the other hand, sulfur, an embrittling impurity, tends to segregate more strongly to cavity surfaces than to grain boundaries.

Existing (but previously unconfirmed) theories of solute segregation effects indicate that the segregation behavior exhibited by boron should enhance grain-boundary cohesion and thus inhibit intergranular fracture, in agreement with our observations. The segregation behavior of sulfur, on the other hand, is predicted to lower grain-boundary cohesion and promote intergranular fracture, again in agreement with our observations.

8. The yield stress of B-doped Ni_3Al decreases with increasing grain size produced by long-term annealing at 1000°C. The yield stress obeys the Hall–Petch relation: $\sigma_y = \sigma_{0,y} + k_y\ d^{-1/2}$, with $\sigma_{0,y} = 163$ MPa and $k_y = 8.2$ MPa $cm^{1/2}$. The frictional stress, $\sigma_o y$, divided by an average grain orientation factor, compares favorably with the critical resolved sheer stresses (CRSS) value for {111} planes of Ni_3Al single crystals.

9. The tensile elongation of B-doped Ni_3Al (24% Al was initially independent of grain size and kept constant at a level of about 50%. With an increase in grain size above 110 μm in diameter, the aluminide showed only a moderate drop in ductility, but no change in basic fracture mode, i.e. transgranular fracture persists.

Acknowledgements—The authors wish to thank J. O. Stiegler and C. C. Koch for helpful discussions and M. H. Yoo and R. O. Williams for useful comments on the manuscript. There are alao thanks due to R. A. Padgett for AES, R. S. Crouse for SEM, W. H. Farmer for metallography, T. J. Henson for electron microprobe analysis, E. H. Lee and M. Winsbro for technical assistance, and Lucy Beeler for preparation of the manuscript.

REFERENCES

1. M. Hansen, *Constitution of Binary Alloys*, pp. 119. McGraw-Hill, New York (1958).
2. P. H. Thorton, R. G. Davis and T. L. Johnson, *Metall. Trans.* **1**, 207 (1970).
3. P. A. Flinn, *Trans. T.M.S.-AIME* **218**, 145 (1960).
4. R. G. Davis and N. S. Stoloff, *Trans. T.M.S.-A.I.M.E.* **233**, 714 (1965).
5. E. A. Aitken, *Intermetallic Compounds* (edited by J. H. Westbrook), pp 491–515. Wiley, New York (1967).
6. C. T. Liu and C. C. Koch, *Technical Aspects of Critical Materials used by the Steel Industry*, Vol. IIB, NBSIR 83-2679-9, National Bureau of Standards (1983).
7. E. M. Grala, *Mechanical Properties of Intermetallic Compounds* (edited by J. H. Westbrook), pp. 358. Wiley, New York (1960).
8. R. Moskovich, *J. Mater. Sci.* **13**, 1901 (1978).
9. K. Aoki and O. Izumi, *Trans. Japan Inst. Metals* **19**, 203 (1978).
10. A. V. Seybolt and J. H. Westbrook, *Acta metall.* **12**, 449 (1964).
11. K. Aoki and O. Izumi, *Nippon Kinzoku Gakkaishi* **41**, 170 (1977).
12. C. L. White and D. F. Stein, *Metall. Trans. A* **9A**, 13 (1978).
13. K. Aoki and O. Izumi, *Nippon Kinzaku Gakkaishi* **43**, 1190 (1979).
14. C. T. Liu, C. L. White, C. C. Koch and E. H. Lee, *Proc. Symp. High Temperature Materials Chemistry II* (edited by Munir *et al.*). The Electrochemical Soc. (1983).
15. D. F. Stein, W. G. Johnson and C. L. White, *Grain Boundary Structures and Properties* (edited by G. A. Chadwick and D. A. Smith), pp. 301–351. Academic Press, New York.
16. A. Joshi, *Interfacial Segregation* (edited by W. C. Johnson and J. M. Blakely), pp. 39–109. ASM, Metal Park (1977).
17. G. K. Wehner, *Methods of Surface Analysis* (edited by A. W. Czanderna), Vol. 1, pp. 5–37. Elsevier, Amsterdam.
18. N. S. Stoloff and R. G. Davis, *Prog. Mater. Sci.* **13**, 1 (1966).
19. L. E. Davis, N. C. MacDonald, P. W. Palmberg, G. E. Riach and R. E. Weber, *Handbook of Auger Electron Spectroscopy*, 2nd eds., pp. 1–12, 23, 45, 61, 93, Physical Electronics Industries, Eden Prairie, MN (1976).
20. C. T. Liu, C. L. White and M. Chang, unpublished results, ORNL (1983).
21. C. C. Koch, J. A. Horton, C. T. Liu, O. B. Cavin and J. O. Scarborough, *Proc. 3rd Int. Conf. on Rapid Solidification* (edited by R. Mehrabian), pp. 264–9, NBS, Gaithersburg, Maryland (1982).
22. C. L. White, R. E. Clausing and L. Heatherly, *Metall. Trans. A* **10A**, 683 (1979).
23. S. S. Hecker, D. L. Rohr and D. F. Stein, *Metall. Trans. A* **9A**, 481 (1978).
24. C. T. Liu, H. Inouye and A. C. Schaffhauser, *Metall. Trans. A* **12A**, 993 (1981).
25. H. H. Stadelmaier and A. C. Fraker, *Metall* **16**, 212 (1962).
26. J. D. Schobel and H. H. Stadelmaier, *Z. Metallk.* **53**, 326 (1962).
27. H. H. Stadelmaier, *Developments in the Structural Chemistry of Alloy Phases*, p. 141 Plenum Press, New York (1969).
28. S. Yalisove and W. R. Graham, Univ. of Pennsylvania, private communication, November (1983).
29. D. F. Stein and L. A. Heldt, *Interfacial Segregation* (edited by W. C. Johnson and J. M. Blakely), pp. 239–260. ASM, Metal Park (1977).
30. C. L. White, J. R. Keiser, and D. N. Braski, *Metall. Trans. A* **12A**, 1485 (1981).
31. C. L. Briant and R. P. Messmer, *Phil. Mag. B*-**12**, 569 (1980).
32. R. P. Messmer and C. L. Briant, *Acta metall.* **30**, 457 (1982).
33. D. McLean, *4e Colloque de Metallurgie: Properties des Joints de Grains*. pp. 85–95. Presses Universitaires de France, Paris (1961).
34. D. McLean, *Mechanical Properties of Metals*, pp. 249–250. Wiley, New York (1962).
35. C. J. McMahon Jr and V. Vitek, *Acta metall.* **27**, 507 (1979).
36. M. L. Jokl, V. Vitek, and C. J. McMahon Jr, *Acta Metall.* **28**, 1479 (1980).
37. E. A. Guggenheim, *Thermodynamics: An Advanced Treatment for Chemists and Physicists*, pp. 207–208, North-Holland, Amsterdam (1967).
38. R. J. Asaro, *Phil. Trans. R. Soc. Lond. A* **295**, 151 (1980).
39. E. D. Hondros, *Proc. R. Soc. Lond. A.* **286**, 479 (1965).
40. J. R. Rice, *The Effect of Hydrogen on the Behavior of Metals*, pp. 455–465. Am Inst. Min Engrs, New York (1976).
41. J. P. Hirth, *Phil. Trans. R. Soc. Lond. A* **295** 139 (1980).
42. J. P. Hirth and J. R. Rice, *Metall. Trans. A* **11A**, 1501–1511.
43. R. W. Guard and J. H. Westbrook. *Trans. Am. Inst. Min. Engrs.* **215**, 807 (1959).
44. J. H. Westbrook, *J. Electrochem. Soc.* **104**, 369 (1957).
45. G. F. Hancock, *Physica status solidi* (a)**7**, 535 (1971).

46. K. Aoki and O. Izumi, *Physica status solidi* (*a*) **32**, 657 (1975).
47. O. Noguchi, Y. Oya and T. Suzuki, *Metall. Trans. A* **12**, 1647 (1981).
48. E. O. Hall, *Proc. Phys. Soc., Sect. B* **64**, 747 (1951).
49. N. J. Petch, *J. Iron Steel Inst.* **174**, 25 (1953).
50. A. H. Cottrell, *Trans. Am. Inst. Min. Engrs* **212**, 192 (1958).
51. E. M. Schulsen and J. A. Roy, *Acta metall.* **26**, 29 (1978).
52. L. Y. Popov. E. V. Kozlov and N. A. Aleksendrov, *Fizika Metall. Metalloved.* **21**, 1756 (1966).
53. S. M. L. Sastry, *Mater. Sci. Engng* **22**, 237 (1976).
54. F. M. C. Besag and R. E. Smallman, *Acta metall.* **18** 429 (1968).
55. P. O. Kettunun, *Phil. Mag.* **16**, 253 (1967).
56. R. W. Armstrong *et al. Phil. Mag.* **7**, 45 (1962).
57. L. R. Curwick, *Strengthening Mechanisms in Nickel-Base Superalloys*, Ph.D. Dissertation, University of Minnesota (1972).
58. K. Aoki and O. Izumi, *Acta metall.* **27**, 807 (1979).